https://www.aimspress.com/journal/Math

Research article

Magnesium aluminum spinel for ultrasonic temperature sensing based on guided waves

Haijian Liang[1,2,*], Xinhui Wang[3] and Hongxin Xue[4]

1 State Key Laboratory of Dynamic Measurement Technology, North University of China, Taiyuan，Shanxi 030051, China
2 School of Software, North University of China, Taiyuan, Shanxi 030051, China
3 Department of Computer Science, Taiyuan Normal University, Taiyuan 030619, China
4 School of Computer Science and Technology, North University of China, Taiyuan, Shanxi 030051, China

* **Correspondence:** Email: 20230128@nuc.edu.cn.

Abstract: Sensors are crucial for measuring combustion temperatures in aerospace and aviation engine testing. However, current sensors have poor oxidation resistance, low impact resistance, limited lifespan, and inadequate temperature measurement accuracy, often resulting in unsatisfactory testing outcomes. New sensor designs are urgently needed to address these issues. We propose a new sensor with advanced materials and technologies, based on the principle of ultrasonic guided wave temperature measurement with magnesium aluminum spinel ($MgAl_2O_4$) and magnesium-doped aluminum oxide crystals as ultrasonic waveguides. The design parameters of this sensor's sensitive elements were meticulously crafted. Finite element method simulations were then conducted to assess the impact of groove depth on ultrasonic propagation characteristics. Ultrasonic temperature sensors with spinel and magnesium-doped aluminum oxide were fabricated via the laser heated pedestal growth method. These sensors were calibrated in an oxidative environment, demonstrating a temperature sensitivity of 0.48 m/s·°C and a repeatability of 95% across a range from 20 °C to 1600 °C. By comparison among the three materials at a constant temperature, the sound velocity of sapphire was the fastest, followed by magnesia-doped alumina, while magnesia-alumina spinel was slowest. Thus, magnesia-alumina spinel can be considered an effective acoustic waveguide material for facile signal acquisition and high-temperature resolution. The proposed sensor design shows promise for applications in environments prone to oxidative erosion and high temperatures, offering an innovative solution for reliable temperature measurement within the harsh environments of aerospace and aviation engines.

---

1. Introduction

Contact and non-contact temperature measurement methods are commonly used to measure internal temperatures in aerospace and aviation engines. Contact methods, which are suitable below 1600°C, include thermocouples, temperature-indicating paints, crystal-based techniques, and optical fibers [1]. Non-contact methods include thermal imaging cameras and multispectral approaches [2,3]. Though effective, contact methods are limited to shorter-term applications in oxidizing environments at temperatures exceeding 1600 °C. Measuring rakes made of platinum-rhodium thermocouples, for example, can be used only for brief durations in oxidizing environments above 1600 °C, such as temperature measurements in engine combustion chambers [4–6]; furthermore, the precious metals necessary to fabricate these thermocouples are very costly. Temperature-indicating paints and crystal temperature measurement techniques are effective but only within engine combustion chambers and blades at maximum environmental temperatures and they cannot be used to measure temperature changes in real-time [7–9]. Optical fibers are significantly affected by ambient light in the testing environment, rendering measurements inaccurate when temperatures exceed 1300 °C [10]. Non-contact measurement methods also have significant limitations. Changes in emissivity, as well as factors, such as moisture and dust in the exhaust gas, can affect their accuracy [11].

Traditional measurement methods do not perform effectively in high-temperature oxidizing environments, such as those of aircraft engines, where extreme temperatures can cause turbine blades and other components to burn out. Accurately measuring internal temperatures in aerospace engines is crucial for optimizing structural designs, minimizing redundancy, and improving overall performance. There is demand for new types of sensors capable of long-term operation in oxidizing environments at temperatures over 1600 °C to enable accurate temperature measurements in harsh environments, such as those of aero-engine turbine blades and the interiors of rocket engines.

Ultrasonic temperature measurement technology is a novel method based on the propagation of ultrasonic waves through a medium, where the speed of sound changes with the environmental temperature. This relationship between sound speed and temperature allows for accurate temperature measurement to nearly the melting point of the material [12]. In recent years, magnesium aluminate spinel (*MgAl₂O₄*, referred to hereafter simply as "spinel") has been widely used in high-temperature furnace windows and high-temperature sensor substrates. It is favored for its excellent thermal, mechanical, and optical properties. The development of laser-heated pedestal growth (LHPG) technology for growing single crystals [13–15] further allows for the development of spinel ultrasonic waveguides with high length-to-diameter ratios at lengths greater than 100 mm and diameters below 1 mm. Thus, the erosion resistance, oxidation resistance, and high-temperature stability of spinel can be leveraged to take long-term, real-time temperature measurements in oxidative environments above 1600 °C.

2. Basic principles

2.1. Principle of ultrasonic guided wave temperature measurement

Ultrasound has good directionality and anti-interference properties, making it highly suitable for measuring temperatures in challenging environments. Applying ultrasonic guided waves enhances both the measurement range and the resistance to electromagnetic interference under oxidative conditions [16,17].

When ultrasound propagates through materials, its speed c has a certain correlation with temperature T [18–20]. In solid media, the longitudinal and transverse wave speeds of ultrasound can be expressed as follows:

$$v_L = \sqrt{\frac{E(1-\rho)}{\rho(1+\sigma)(1-2\sigma)}} \tag{1}$$

$$v_S = \sqrt{\frac{E}{2\rho(1+\sigma)}} \tag{2}$$

where v_L represents the longitudinal wave speed of ultrasound, v_S is the transverse wave speed of ultrasound, E is the elastic modulus of the selected waveguide material, ρ is the density of the material, and σ is Poisson's ratio. Typically, the relationship between the longitudinal wave speed of ultrasound and temperature is utilized for temperature measurement; accordingly, this equation can be transformed into Eq (3).

$$v(T) = \sqrt{\frac{E(T)}{\rho(T)}} \tag{3}$$

The speed of ultrasound can be calculated by measuring its propagation time t and determining the gauge length l of the sensitive region, thus revealing the relationship between the speed of sound $v(T)$ and the ambient temperature T, as expressed in Eq (4).

$$\Delta t(T) = \frac{2l}{v(T)} \tag{4}$$

The speed of the sound corresponding to the temperature can be determined by measuring the propagation time of the ultrasound. In the proposed equipment setup, an upper computer sends an excitation signal to an ultrasonic excitation power supply, which generates a pulse excitation. This excites an acoustic signal at an ultrasonic probe coupled to an ultrasonic waveguide. As the ultrasound encounters the prepared sensitive structure, the reflected acoustic signal reaches the probe and is converted into an electrical signal. A data acquisition system transmits this amplified signal to the upper computer for processing, calculation, and display, thereby achieving the measurement of ultrasound propagation time and determining the speed of sound corresponding to the temperature. The testing principle is illustrated in Figure 1.
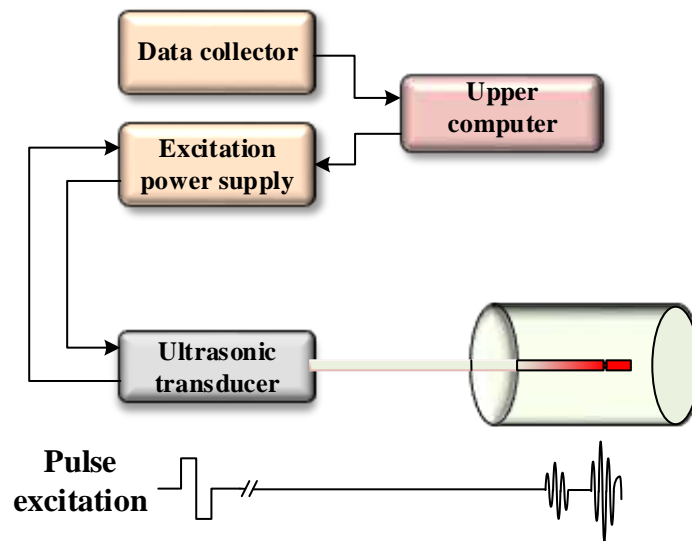
Figure 1. Test schematic diagram.

2.2. Principle of acoustic impedance matching

A key parameter of the sensor's sensitive element is the reflection coefficient, which is related to the impedance matching of the acoustic wave transmission. Acoustic wave reflection occurs when transmitted ultrasonic waves encounter a change in the diameter of the waveguide rod, a phenomenon closely related to changes in acoustic impedance [21]. The acoustic impedance at the location where the acoustic wave reflection occurs can be expressed as follows:

$$Z = \rho c A \tag{5}$$

and the formulas for the reflection coefficient R and transmission coefficient T at the sensitive element section are:

$$R = \frac{Z_2 - Z_1}{Z_2 + Z_1} \tag{6}$$

$$T = \frac{2Z_2}{Z_2 + Z_1} \tag{7}$$

where Z_1 and Z_2 represent the impedances before and after the change in diameter, respectively. The relationship between Z_1 and Z_2 is expressed in Eq (8):

$$\frac{Z_1}{Z_2} = \frac{d_1^2}{d_2^2} \tag{8}$$

where d_1 is the initial diameter of the sensitive element (i.e., diameter of the waveguide rod) and d_2 is the diameter after the change at that section. By substitution into Eq (8), R and T can be further expressed as:

$$R = \frac{d_2^2 - d_1^2}{d_2^2 + d_1^2} \tag{9}$$

$$T = \frac{2d_2^2}{d_2^2 + d_1^2} \tag{10}$$

Similarly, the diameter ratio at the variable cross-section can be obtained from the reflection coefficient T of the sensitive element:

$$\frac{d_2}{d_1} = \sqrt{\frac{1+R}{1-R}} \tag{11}$$

Selecting a reasonable reflection coefficient is essential for constructing an ideal sensitive structure that combines a high signal-to-noise ratio, high sensitivity, and robust interference resistance. To minimize ultrasound dispersion and ensure the structural integrity of the sensor's waveguide rod, a spinel waveguide material with a diameter of 0.7 mm and a groove diameter of 0.57 mm was chosen for the proposed design. This effectively improves the signal-to-noise ratio, reduces the difficulty of signal acquisition and processing, and enhances measurement accuracy. The section length was designed as 25 mm according to Eq (4), balancing the necessity for a minimal section length with the difficulty of signal acquisition and processing.

## 3.   Simulation analysis of ultrasonic transmission characteristics

The diameter of the sensor's waveguide rod, the length and diameter of the sensitive element section, and other parameters (e.g., width) were determined by theoretical analysis. To validate these theoretical values and refine the sensor's design, finite element software was employed to simulate the ultrasound transmission within the waveguide rod; this helped in visualizing the ultrasound transmission characteristic curves and optimizing the structure of the sensor. A spinel simulation structure was constructed for this purpose. Its parameters are listed in Table 1.

Table 1. Sensor simulation parameters.

Length	Diameter	Section length	Groove diameter	Reflection coefficient
300 mm	0.7 mm	25 mm	0.57 mm	0.2

The simulation results, as shown in Figure 2, indicated clear echoes at specific sections and the end of the waveguide rod, including secondary echoes. These confirm the viability of the proposed method for ultrasound signal detection. The section diameter was subsequently adjusted to 0.4 mm for additional simulations to explore the impact of different groove diameters on sensor signals. There was a significant increase in the amplitude of the echo signal at the section position, albeit with a slight decrease at the end wave echo. While the enhanced section echo signal is beneficial, the increased groove depth reduces the overall resistance to thermal shock and vibration, which would compromise its long-term durability. When the groove depth was designed to be 0.65mm, it will have a greater
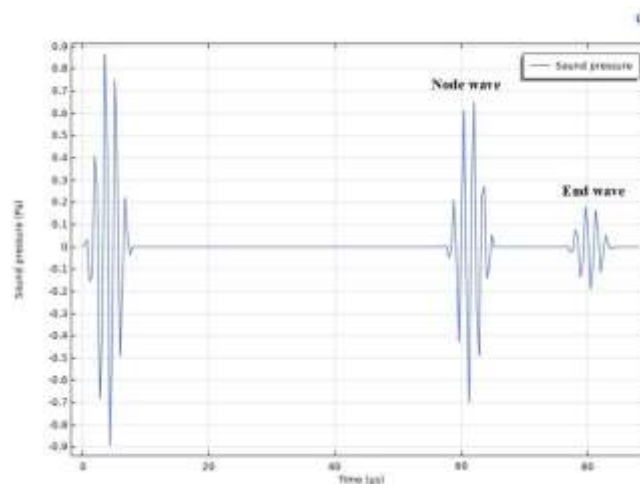
amplitude in the echo signal, and the amplitude of the end wave decreases. Thus, the groove depth must be carefully designed to balance signal clarity with structural integrity.
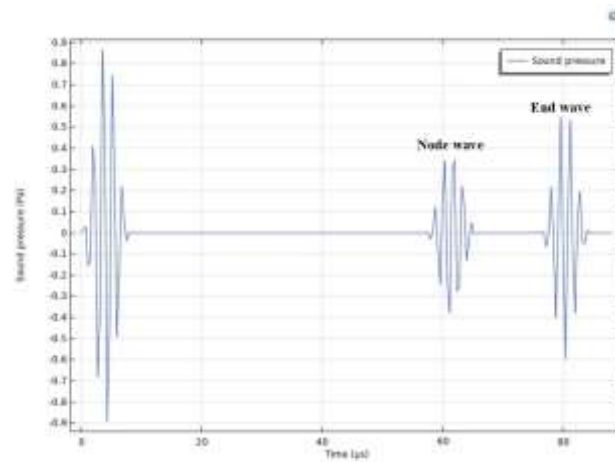
（a）
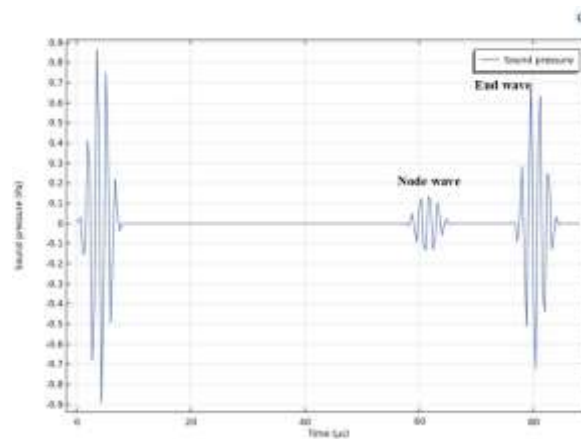
（b）

（c）

Figure 2. Simulation of ultrasonic propagation characteristics: (a)the groove diameter is 0.57 mm, (b) the groove diameter is 0.4 mm, and (c) the groove diameter is 0.65 mm.

Additional simulations were conducted to examine the ultrasound propagation characteristics across different temperatures, producing a relationship curve between the speed of sound and temperature (Figure 3). The speed of sound in the spinel gradually decreased as the temperature increased, from 9261 m/s at room temperature to 8569 m/s at 1600°C, demonstrating a clear monotonous decreasing trend that corroborates the theoretical predictions.
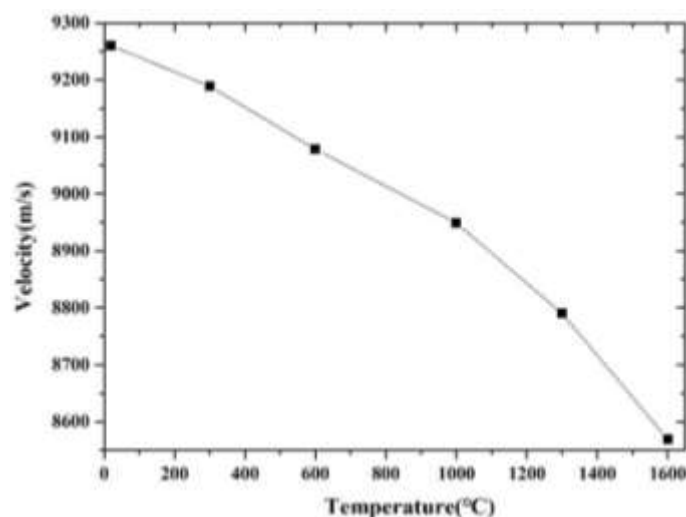

Figure 3. Simulated relationship between temperature and speed during ultrasonic propagation.

4. Sensor fabrication and temperature measurement system construction

4.1. Waveguide growth

In recent years, significant progress has been made in the research of functional crystal materials. These materials are becoming more widely used in the sensor industry as main materials, substrates, and infrared window components. Spinel materials, which have melting points as high as 2150 °C, possess excellent thermal, mechanical, optical, and electrical properties.

Spinel performs similarly to the more commonly used sapphire, with properties including a thermal expansion coefficient of 7.33×10^{-6}/ °C, a melting point of 2135 °C, and a Mohs hardness of 8.5. In comparison, alumina has a melting point of 2050 °C, a Mohs hardness of 9, and a thermal expansion coefficient of 7.5×10^{-6}/ °C. However, spinel has superior chemical stability and, due to its cubic structure and optical isotropy, is an ideal material for transparent substrates and sublayers. These performance characteristics are outlined in Table 2.

Table 2. Spinel versus sapphire.

Category	Molecular formula	Melting point (℃)	Elastic modulus (GPa)	Poisson's ratio	Density (g/cm³)
Spinel	$MgAl_2O_4$	2135	273	0.26	3.58
Sapphire	$\alpha\text{-}Al_2O_3$	2050	344	0.23	3.97

The LHPG method is extensively used to grow high-quality single-crystal fibers, particularly in producing ultrasonic waveguides. Control over the pulling speed of the seed crystal during the growth process is crucial for successfully fabricating such waveguides. This parameter significantly influences both ultrasonic transmission and the sensitivity of sensing elements to environmental temperatures.

To operate the proposed method, a focused laser is used to heat the source rod to create a molten zone into which the seed crystal is inserted. The geometric parameters of the single-crystal ultrasonic waveguide are regulated by adjusting the pulling speed of the seed crystal v_c and the rising speed of the source rod v_r, allowing the growth of single-crystal waveguides with specific diameters tailored to the needs of the application at hand. A schematic diagram illustrating this growth apparatus is shown in Figure 4.
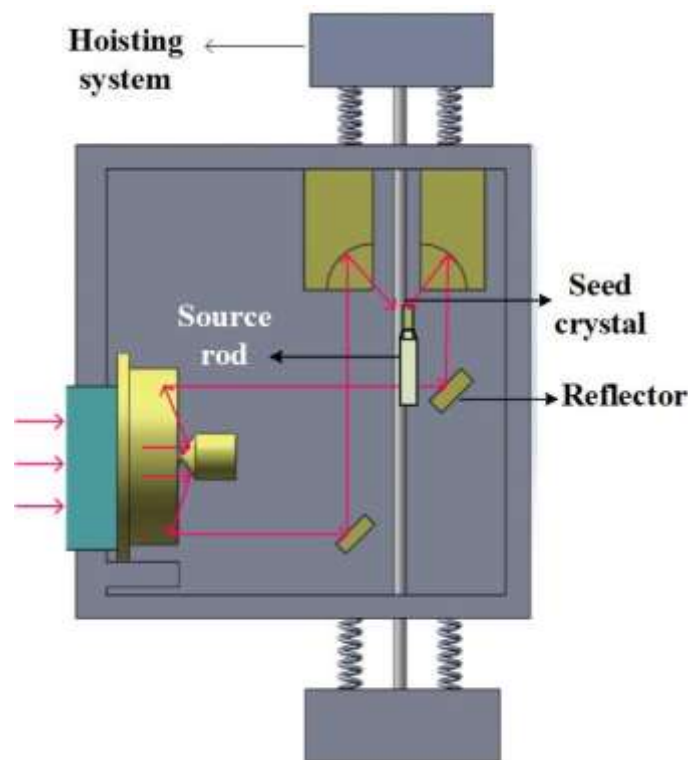

Figure 4. Single crystal fiber growth device.

To grow an ultrasonic waveguide with a uniform shape and no undulations, the pulling speed of the seed crystal v_c and the rising speed of the source rod v_r should satisfy the following relationship:

$$\frac{v_c}{v_r} = \left(\frac{D_c}{D_r} \right)^2 \tag{12}$$

where D_c represents the diameter of the seed crystal and D_r is the diameter of the source rod.

In this study, a high aspect ratio ultrasonic waveguide single-crystal fiber with a length of 300 mm and a diameter of 0.7 mm was grown using a spinel waveguide seed crystal, as illustrated in Figure 5.
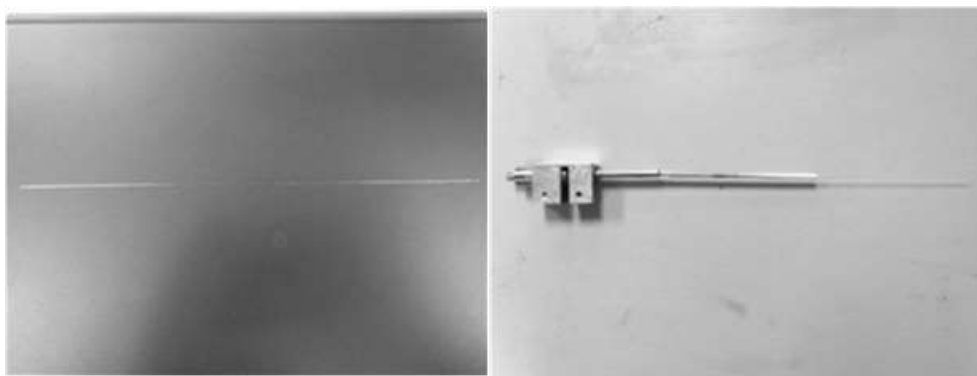
Figure 5. Growth of spinel ultrasonic waveguide.

4.2. Construction and testing of the ultrasonic temperature measurement system

An innovative system was constructed in this study based on the principle of ultrasonic temperature measurement. The system consists of a temperature-sensitive element, an ultrasonic transmitting and receiving device, an ultrasonic signal acquisition and processing system, and a probe coupling device, as depicted in Figure 6.

The temperature-sensitive element was manufactured using precision engraving methods to form a temperature-sensitive structure. A CTS-8077PR pulse transmitter-receiver was used for the transmission and reception of ultrasound, employing a 2.5 MHz ultrasonic probe. This setup facilitated the accurate capture of echo signals, which were then processed to extract characteristic wave signals to compute the ultrasonic propagation time. The system was evaluated using a high-temperature resistance furnace capable of providing a controlled temperature range from 20°C to 1600°C. Readings were taken at 100°C intervals throughout the testing process, with each point maintained for 10 min to ensure equilibrium between the sensor temperature and ambient conditions before proceeding with signal acquisition. A standard platinum-rhodium thermocouple was used as the reference temperature standard for calibration purposes.
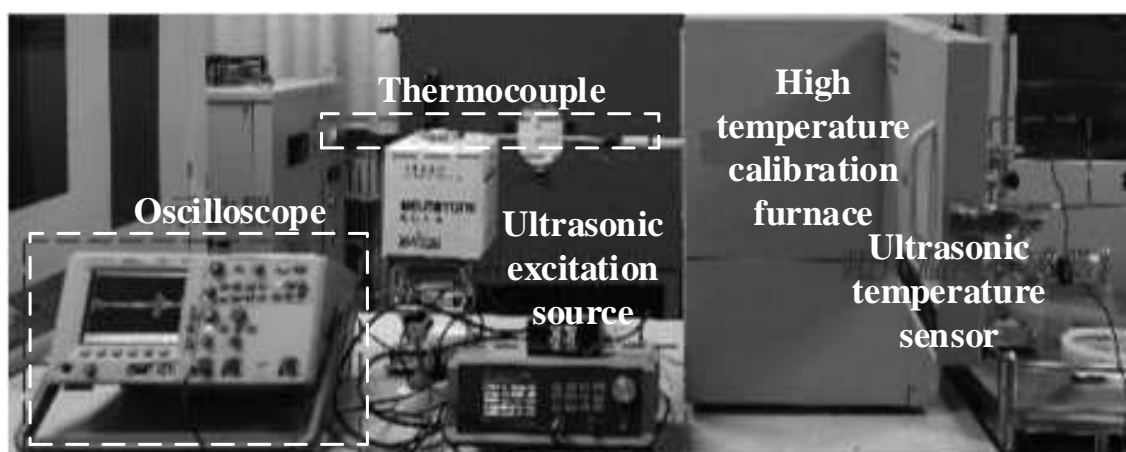

Figure 6. An ultrasonic temperature measuring system.

4.3. Algorithm

The ultrasonic signals were initially processed to remove the DC component. After conducting multiple experiments, a sliding window length of 9 was found to yield the optimal filtering effect. The echo signal's spectrum exhibited bandpass characteristics. The passband center frequency was set to 2.5 MHz to match the center frequency of the ultrasonic transducer. For enhanced computational efficiency and speed, convolution operations were executed using both FFT and IFFT algorithms. The relationship between the node wave and the endpoint wave was established using their cross-correlation function based on their correlation and time difference [22]. The time delay was identified by the peak value in the cross-correlation curve, which reflects the delay between the two signals. The ultrasonic delay time was then calculated by dividing the number of sampling points from the starting point to this peak by the sampling frequency. Since the node wave and end point are positively correlated, a correlation coefficient of 1 was assigned. This algorithm boasts high accuracy, rendering it well-suited for ultrasonic signal processing; however, it incurs substantial computational demands and requires extended computation times. To perform fast calculations on the upper computer, the algorithm has been simplified to reduce computational complexity and speed up the computation. However, when measuring continuously, if the amount of data is too large, the calculation speed is a bit slow. A flowchart of this algorithm is presented in Figure 7, and the parameters of the algorithm are listed in Table 3.

Table 3. Algorithm parameters.

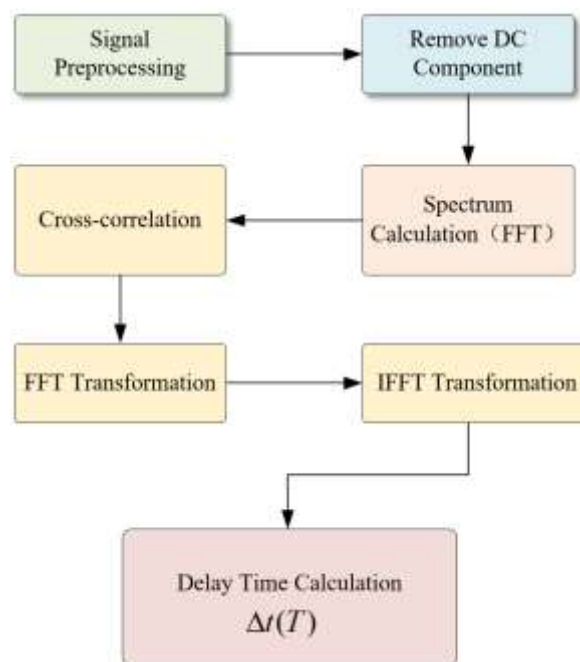| Parameters	Sliding window length	Center frequency	Correlation coefficient
Value	9	2.5MHz	1

Figure 7. Algorithm flowchart.

5. Results and analysis

The LHPG method was used to prepare spinel and magnesium-doped alumina ultrasonic waveguides. Ultrasonic temperature sensors were created from these materials and each was subjected to three round-trip tests. The resultant data were analyzed using specialized algorithms to determine the ultrasonic propagation time, allowing for calculating the relationship between ultrasonic propagation temperature and velocity. The average sensitivity and repeatability of the sensors were also evaluated.

For the spinel ultrasonic sensor, three cycles of heating and cooling tests revealed temperature-velocity and temperature-delay time relationship curves within the temperature range of 20 °C to 1600 °C, as shown in Figure 8. As the temperature increased during the forward tests, the ultrasonic propagation speed in the spinel decreased from 9250 m/s to 8500 m/s, and the propagation time increased from 5.4 μs to 5.85 μs (Figure 8(a), Figure 8(b)). During the backward tests, as the temperature decreased, the ultrasonic propagation speed in the spinel increased from 8500 m/s to 9250 m/s and the propagation time recovered from 5.85 μs to 5.4 μs (Figure 8(c), Figure 8(d)). These trends in velocity and propagation time are consistent with the simulation results.
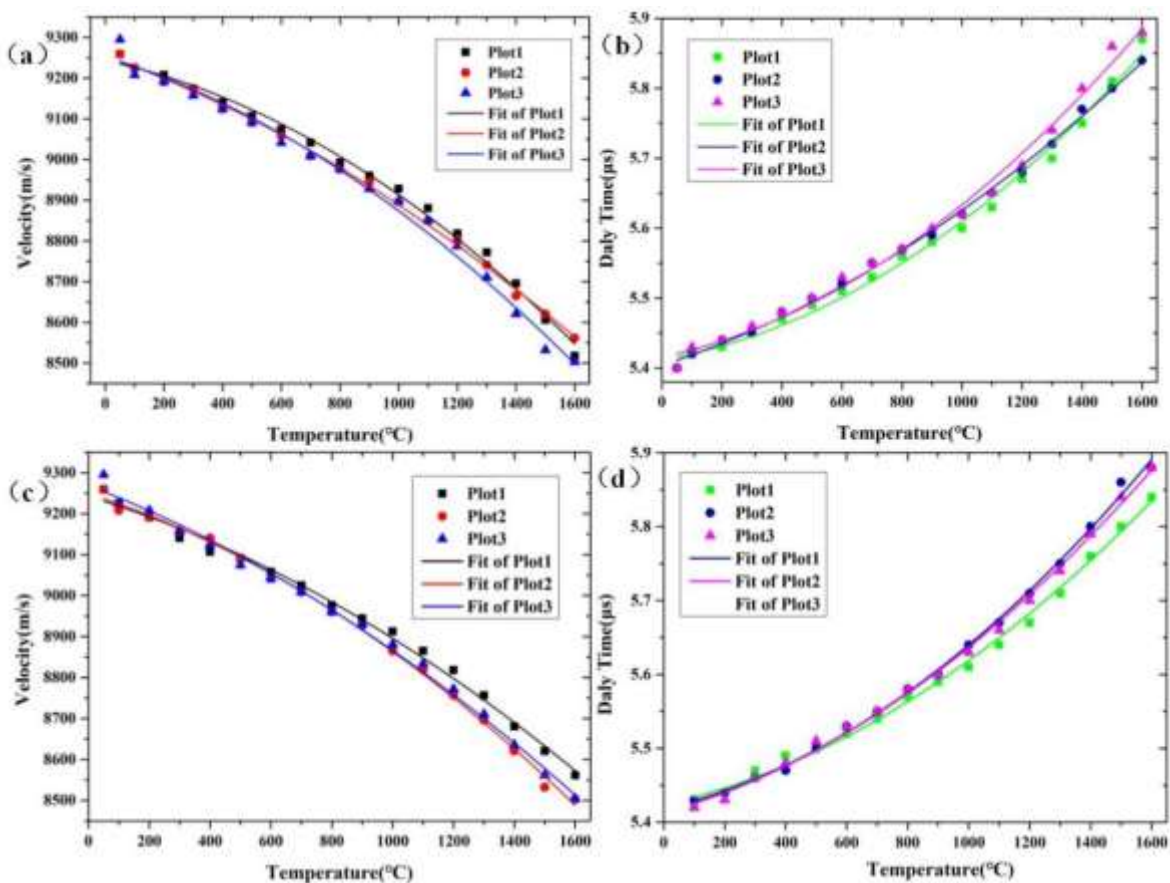

Figure 8. Temperature-sound velocity curve of self-made ultrasonic waveguide.

Based on Formulas (13) and (14), the sensitivity of the sensor was calculated to be 0.48 m/s·°C with a repeatability of 95%.

Average sensitivity:

$$s = \frac{Y_{max} - Y_{min}}{X_{max} - X_{min}} \tag{13}$$

Repeatability:

$$\xi_R = \frac{cS_{max}}{Y_{FS}} \times 100\% \tag{14}$$

Similar forward and backward tests were also conducted for the magnesium-doped alumina ultrasonic sensor. Temperature-velocity and temperature-delay time relationship curves for the sensor were obtained within the temperature range of 50°C to 1600°C, as shown in Figure 9. During the forward tests, as the temperature increased, the ultrasonic propagation speed in the spinel decreased from 10505 m/s to 9551 m/s, and the propagation time increased from 5.15 μs to 5.65 μs (Figure 9(a), Figure 9(b)). As the temperature decreased during the backward tests, the ultrasonic propagation speed in the spinel increased from 9551 m/s to 10505 m/s, and the propagation time recovered from 5.65 μs to 5.15 μs (Figure 9(c), Figure 9(d)). These trends in velocity and propagation time are also consistent with the simulation results. Based on Formula (13, 14), the sensitivity of the sensor was calculated to be 0.615m/s·°C, with a repeatability of 97%.
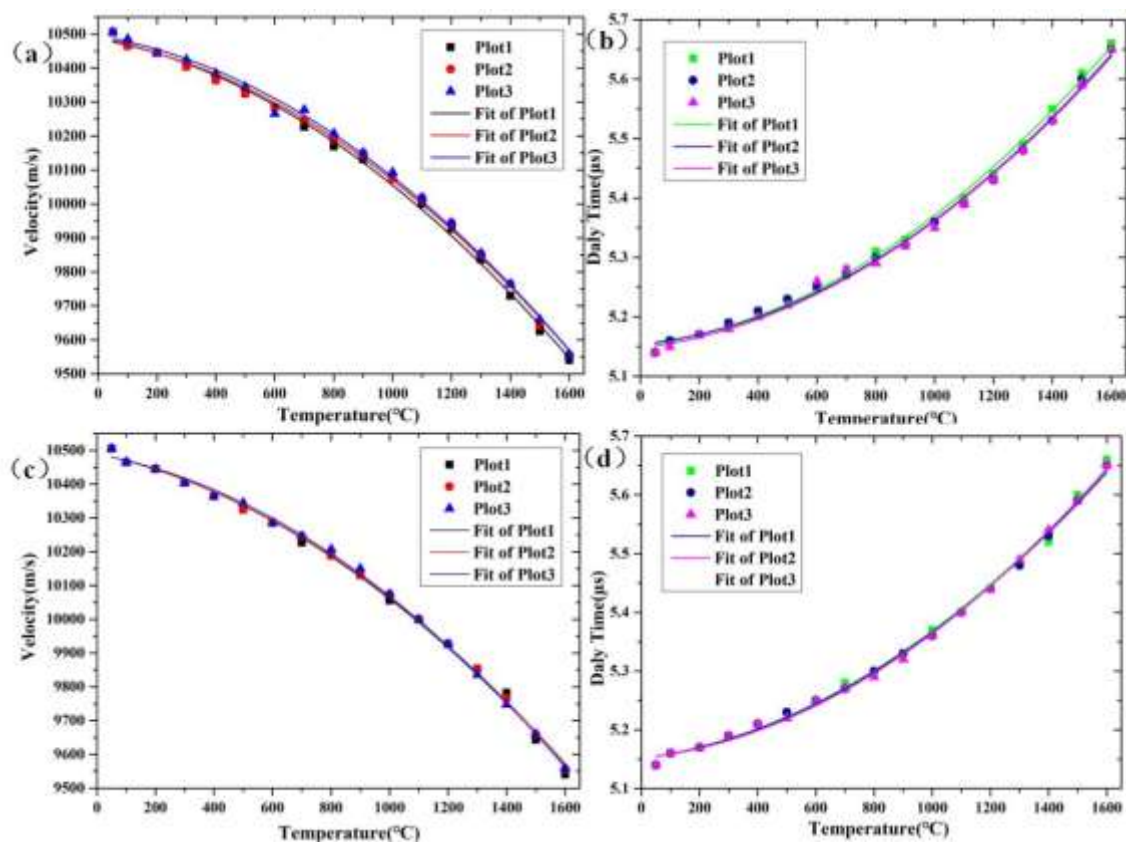

Figure 9. Magnesium-doped alumina.

As per comparisons of the transmission characteristics of ultrasonic guided waves in spinel and magnesium-doped alumina, the magnesium-doped alumina waveguide exhibited less noise in the acoustic signal compared to the spinel material under identical filtering conditions. At a temperature of 1600°C, the amplitude of the spinel acoustic waveguide remained almost unchanged compared to that at 50°C, while the amplitude of the magnesium-doped alumina acoustic waveguide decreased by approximately 70%. However, at high temperatures, the spinel waveguide produced more distinguishable signal waveforms. The magnesium doping in alumina introduced instability that increased the acoustic impedance within the crystal at elevated temperatures, resulting in a noticeable decrease in signal waveform amplitude at higher temperatures compared to lower ones. This complicated the extraction of temperature signals, as depicted in Figure 10. Researchers should focus on enhancing the stability of magnesium doping in these applications in the future.
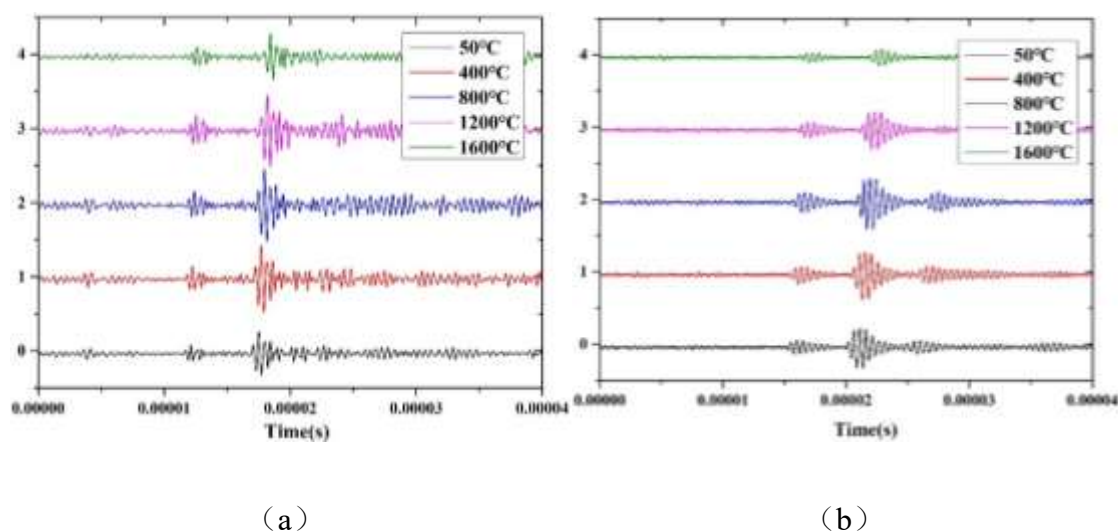

（a）　　　　　　　　　　　（b）

Figure 10. Ultrasonic characteristics of spinel and magnesia-doped alumina at different temperatures: (a) Spinel and (b) Magnesia-doped alumina.

Tests conducted within the temperature range of 20 °C to 1600 °C for three types of crystal ultrasonic waveguides (sapphire, magnesium-doped alumina, and spinel) revealed variations in ultrasonic velocities at different temperatures, as shown in Figure 11. From 50°C to 1600°C, the ultrasonic propagation speed of spinel decreased from 9271 m/s to 8527 m/s, the ultrasonic propagation speed of magnesium-doped alumina decreased from 10505 m/s to 9551 m/s, and the sound velocity of sapphire decreased from 10666 m/s to 10000 m/s.

The overall trend indicates a general decrease in sound velocity with increasing temperature. Sapphire exhibited the highest velocity, followed by magnesium-doped alumina, while spinel showed the lowest velocity at equivalent temperatures. While the difference in sound velocity between magnesium-doped alumina and pure alumina was initially slight, it became more pronounced as temperature increased. At the same temperature and acquisition frequency, a lower sound velocity can help to reduce the length of the cell segment, thus facilitating sensor miniaturization.
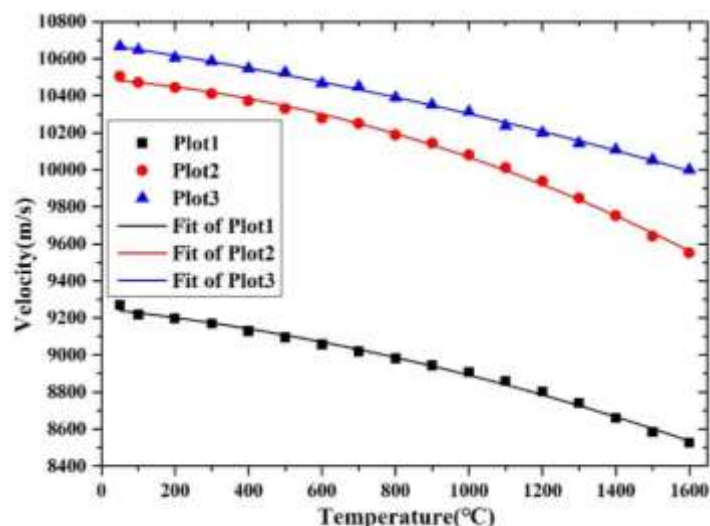
Figure 11. Spinel (Plot 1); Magnesium-doped sapphire (Plot 2); and Sapphire (Plot 3).

6. Conclusions

Temperature measurement in challenging environments, such as in aviation and aerospace engines, is a pressing issue that requires innovative solutions. Based on the principle of ultrasonic temperature sensing, structural parameters for a magnesium-aluminum spinel ultrasonic temperature sensor were designed in this study. The proposed design includes a waveguide diameter of 0.7 mm, a section length of 25 mm, and a groove diameter of 0.57 mm. Simulations of ultrasonic propagation characteristics at different temperatures revealed a decreasing trend in sound velocity with increasing temperature. A magnesium-aluminum spinel ultrasonic waveguide was grown using the LHPG method, then an ultrasonic temperature sensor was fabricated according to the designed parameters. Calibration results demonstrated a sensitivity of 0.48 m/s·°C and repeatability of 95% within the temperature range of 20 °C to 1600 °C.

Comparative analysis of ultrasonic characteristics among magnesium-doped alumina, single-crystal alumina, and magnesium-aluminum spinel revealed a gradual decrease in sound velocities. At the same temperature, single-crystal alumina exhibited the highest sound velocity, followed by magnesium-doped alumina, while magnesium-aluminum spinel had the lowest. Utilizing magnesium-aluminum spinel as an ultrasonic waveguide material can effectively reduce sound velocity, improve the sensor's resolution, and simplify the processing of ultrasonic signals. By leveraging ultrasonic temperature sensing combined with the oxidation resistance of oxide single-crystal materials, there is significant potential to develop an effective solution for high-temperature measurement in the highly oxidizing and highly abrasive environments typical of aviation and aerospace engines.

Author contributions

H. J. Liang: systems design, conceptualization, simulation analysis, data curation, writing-original draft; X. H. Wang: data curation, experimental design, writing-review and editing; H. X. Xue: algorithm design, writing-review and editing. All authors have read and agreed to the published version of the article.

Use of AI tools declaration

Acknowledgments

Conflict of interest

All authors declare no conflicts of interest in this paper.

References

1. K. S. Jhajj, E. Caron, N. L. Chester, K. J. Daun, Accuracy of the rmo couples in transient surface temperature measurements dom-inated by radiant heating, *ASME Paper IMECE*, 2014, 38243. https://doi.org/10.1115/IMECE2014-38243

2. T. B.O. Rockett, N. A. Boone, R. D. Richards, J. R. Willmott, Thermal imaging metrology using high dynamic range near-infrared photovoltaic-mode camera, *Sensors*, **21** (2021), 6151. https://doi.org/10.3390/s21186151

3. S. Zheng, L. Ni, H. Liu, H. Zhou, Measurement of the distribution of temperature and emissivity of a candle flame using hyperspectral imaging technique, *Optik*, **183** (2019), 222–231. https://doi.org/10.1016/j.ijleo.2019.02.077

4. J. V. Pearce, A. D. Greenen, A. Smith, C. J. Elliott, Relating composite- on and thermoelectric stability of Pt–Rh alloy thermocouples, *Int. J. Thermophys*, **38** (2017), 1–12. https://doi.org/10.1007/s10765-016-2132-3

5. J. Deng, W. Wang, L. Hui, J Zhang, X. Jin, A through-hole lead connection method for thin-film thermocouples on turbine blades, *Sensors*, **19** (2019), 1155–1166. https://doi.org/10.3390/s19051155

6. F. Edler, Scaling of thermoelectric inhomogeneities with temperature in platinum-rhodium alloyed thermocouples, *Metrologia*, **60** (2023), 035005. https://doi.org/10.1088/1681-7575/acd3f5

7. Y. F. Ruan, P. F. Wang, L. Huang, W. Zhu, High-temperature sensor based on neutron-irradiated 6H-SiC, *Key Eng. Mater.*, **495** (2012), 335–338. https://doi.org/10.4028/www.scientific.net/KEM.495.335

8. J. Davidsson, V. Ivady, R. Armiento, T. Ohshima, N. T. Son, A. Gali, et al., Identification of divacancy and silicon vacancy qubits in 6H-SiC, *Appl. Phys. Lett.*, **114** (2019), 1–5. https://doi.org/10.1063/1.5083031

9. H. J. Liang, F. B. Yang, L. Yang, Z. Liu, G. Wang, Y. Wei, et al., Research and implementation of a 1800 °C sapphire ultrasonic thermometer, *J. Sensors*, 2017, 9710763. https://doi.org/10.1155/2017/9710763

10. A. Campanellc, A. Morana, S. Girard, A. Guttilla, F. Mady, M. Benabdesselam, et al., Combined temperature and radiation effects on radiation-sensitive single-mode optical fibers, *IEEE T. Nucl. Sci.*, **67** (2020), 1643–1649. https://doi.org/10.1155/2017/9710763

11. T. S. Balamurugan, C. V. Krishnamurthy, A. Kavitha, Non-contact in situ microwave material measurements for high temperature process monitoring, *Rev. Sci. Instrum.*, **90** (2019), 034702.

12. Y. L. Wei, H. J. Liang, G. Wang, W. Xingqi, L. Yang, H. Zhou, et al., Ultrasonic thermometric measurement system for solid rocket combustion chambers, *Ultrasonics*, **113** (2021), 106361. https://doi.org/10.1016/j.ultras.2021.106361

13. C. N. Liu, T. H. Wang, T. S. Rou, N. K. Chen, S. L. Huang, W. H. Cheng, Higher gain of single-mode Cr-doped fibers employing optimized molten-zone growth, *J. Lightwave Technol.*, **35** (2017), 4930–4936. https://doi.org/10.1109/JLT.2017.2767567

14. R. Jorge-enrique, J. E. F. S. Rodrigues, C. H. Antonio, Monocrystalline fiber growth technique: new critical radius considerations, *J. Cryst. Growth*, **570** (2021), 126199. https://doi.org/10.1016/j.jcrysgro.2021.126199

15. F. Rey-garcía, R. Ibáñez, L. A. Angurel, F. M. Costa, G. F. de la Fuente, Laser floating zone growth: overview, singular materials, broad applications, and future perspectives, *Crystals,* **11** (2021), 38. https://doi.org/10.3390/cryst11010038

16. Y. Wei, G. Wang, Y. Gao, Z. Liu, L. Xu, M. Tian, et al., A measurement system of high-temperature oxidation environment with ultrasonic Ir0.6Rth0.4 alloy thermometry, *Ultrasonics*, **89** (2018), 102–109. https://doi.org/10.1016/j.ultras.2018.04.001

17. T. Wang, J. Zhang, L. Yang, G. Wang, H. Wang, N. Zhang, et al., Fabrication and sensitivity optimization of garnet crystal-fiber ultrasonic temperature sensor, *J. Mater. Chem. C*, **8** (2020), 3830–3837. https://doi.org/10.3390/cryst11010038

18. Y. L. Wei, Y. B. Gao, Z. Q. Xiao, G. Wang, M. Tian, H. Liang, Ultrasonic Al_2O_3 ceramic thermometry in High-Temperature oxidation environment, *Sensors*, 2016.

19. N. R. Skov, J. S. Bach, B. G. Winckelmann, H. Bruus, 3D modeling of acoustofluidics in a liquid-filled cavity including streaming, viscous boundary layers, surrounding solids, and a piezoelectric transducer, *AIMS Math.*, **4** (2019), 99–111. https://doi.org/ 10.3934/Math.2019.1.99

20. T. Y. Wong, Y. Tang, F. Zou, Z. Su, An Ultra-High accuracy temperature measurement method using acoustic waveguide, *IEEE Sens. J.*, **21** (2021), 2618–2626. https://doi.org/10.1109/JSEN.2020.3022518

21. Y. Dong, Q. Yue, D. Cheng, Z. Zhou, R. Liang, X. Dong, Ultrasonic transducer with BiScO3-PbTiO3-based ceramics of operating temperature over 400 °C, *Sensors Actuat. A-Phys.*, **340** (2022), 113528. https://doi.org/10.1016/j.sna.2022.113528

22. A. Mokhtari, Time-Delay estimation of ultrasonic testing signals by a combination of cross correlation and response surface method, *Mater. Eval.,* **76** (2018), 185–191.